Non-linear MHD modelling of Edge Localized Modes suppression by Resonant Magnetic Perturbations in ITER.

M. Becoulet (marina.becoulet@cea.fr;), G.T.A. Huijsmans, C. Passeron
CEA, IRFM
13108 Saint-Paul-Lez-Durance, France

Y.Q. Liu, T. E. Evans*, L. L. Lao
General Atomics, PO Box 85608, San Diego, CA 92186-5608, USA
*Deceased

L. Li
Donghua University1882 Yan'an Road West, Shanghai, China, 200051

A. Loarte, S. Pinches, A. Polevoi, M. Hosokawa
ITER Organization, Route de Vinon-sur-Verdon - 13067 St Paul Lez Durance, France

S K Kim
Princeton Plasma Physics Laboratory,PO Box 451, Princeton, NJ 08540,USA.

S.J.P. Pamela
CCFE, Culham Science Centre, Oxon, OX14 3DB, UK Abingdon, UK.

S. Futatani
Universitat Politècnica de Catalunya
Barcelona, Spain

and JOREK Team
(see in M Hoelzl et al 2020 Nucl. Fus. sub, https://arxiv.org/abs/2011.09120;)

ABSTRACT

Edge Localized Modes (ELMs) suppression by Resonant Magnetic Perturbations (RMPs) was studied with the multi-harmonic non-linear MHD code JOREK for ITER H-mode scenarios *15MA,12.5MA,10MA/5.3T*, obtained by the ASTRA code. RMP spectra, optimized by the linear MHD MARS-F code, with main toroidal harmonics *N=2, N=3, N=4* used as boundary conditions of the computational domain of JOREK including realistic RMP coils, plasma, divertor and wall geometry. The model includes all relevant plasma flows: toroidal rotation, two fluid diamagnetic effects and neoclassical poloidal friction. The threshold for ELM suppression was found at a maximum RMP coils current of *45kAt-60kAt* compared to the coils maximum capability of *90kAt*. With RMPs, the main harmonic and the non-linearly coupled harmonics remain dominant at the plasma edge, producing continuous MHD turbulent transport and suppressing ELMs in all scenarios. In the high beta poloidal steady-state *10MA/5.3T* scenario a rotating QH-mode without ELMs was observed even without RMPs. *N=3* RMPs induced a static QH-like mode, locked to the RMP fields in this scenario. The 3D divertor heat and particle fluxes in the stationary RMP phase show the characteristic splitting with the main RMP toroidal symmetry. The radial extension of the footprints typically was *~20 cm* in inner divertor and *~40 cm* in outer divertor with heat fluxes decreasing further out from the initial strike point from *~5MW/m^2* to *~1MW/m^2* in the stationary regime with RMPs and total power in the divertor *~50MW*. The footprints remain within the divertor target and baffle areas, however with rather small margin in the outer divertor which could be an issue for the first wall especially in transient regimes when part of the plasma thermal energy is released due to switching on the RMP coils.

1. INTRODUCTION

The intensive experimental and theoretical study of ELMs and methods of their control is of great importance for ITER [1, 3]. The application of small external RMPs has been demonstrated to be efficient in the suppression/mitigation of ELMs in present day tokamaks [2]. RMPs are foreseen as the main method of ELMs control in ITER [3]. However, significant progress in understanding of physics of the interaction of ELMs with RMPs is still required to make reliable predictions for next step machines such as ITER and DEMO. The non-linear MHD code JOREK [4] is successfully used to model ELMs mitigation and suppression in present day tokamaks. Recent modelling results of RMP experiments in ASDEX-Upgrade [5] and KSTAR [6] validated in

many aspects the RMPs and ELMs physics models implemented in JOREK code [5-7]. It was demonstrated, in particular, that the non-linear multi-harmonics approach, including a realistic tokamak geometry with the X-point and the Scrape-Off-Layer (SOL), realistic geometry and spectrum of RMP coils, toroidal rotation, the bi-fluid diamagnetic effects and neoclassical poloidal friction represent a minimum model which permits to reproduce experimental results. In particular, it was found that the external kink-peeling plasma response is an important factor for ELM suppression [5] and that the RMP spectrum should be adjusted in this respect. This provides additional support to the new (compared to vacuum [2]) criterion for ELM suppression proposed in [9] where the RMP spectrum is optimized to obtain a maximum displacement near the X-point (kink response) with the linear resistive MHD plasma response provided by the MARS-F code. In the non-linear modelling [6-7], RMPs drive non-linearly coupled side harmonics locked to the static RMP in the ELM suppression stage while strongly mitigating the medium *N*-harmonics responsible for ELM crash. In the present work, the non-linear MHD modelling results of the interaction of ELMs with RMPs in ITER are presented for the first time. Realistic ITER scenarios and geometry including wall, divertor, SOL and RMP coils with the optimum [9, 10] phasing, according to linear MHD MARS-F criterion, were used.

2. INITIAL CONDITIONS

The parameters of ITER H-mode scenarios with the magnetic field B_{tor}=*5.3T* and plasma currents of *15MA, 12.5MA and 10MA* as modelled by the ASTRA code [8] with toroidal flow profiles self-consistently calculated with NBI heating and momentum input, documented in ITER IMAS database (Tab.1), were used as initial conditions. Note that here the two fluid version of JOREK was used but with equal temperatures: $T_i = T_e$. The initial profiles for each ITER scenario studied here are presented in Fig.1.

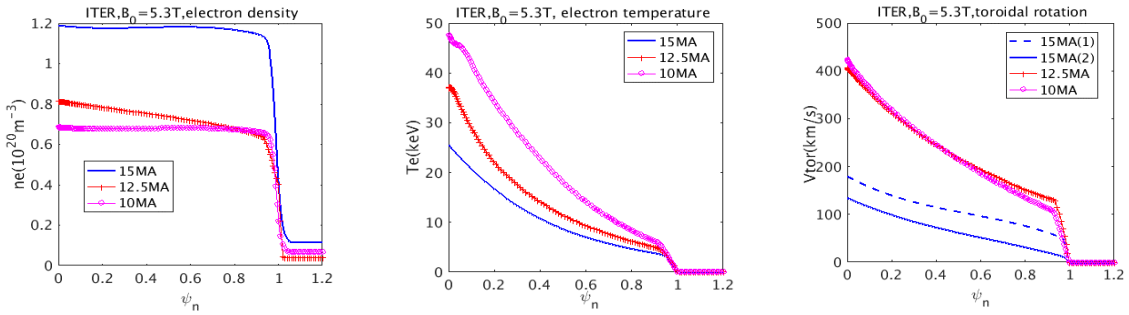


Fig.1. From left to right: initial electron density, electron temperature and rotation profiles used in modelling for different ITER scenarios. Note that for 15MA scenario two rotation profiles were used.

The non-linear MHD code JOREK with relevant flows and RMP model is described in detail in [5-7]. The numerical domain includes closed flux surfaces, X-point and SOL up to the ITER wall. On the divertor targets, Bohm sheath boundary conditions were used for the fluid velocity and the heat flux normal to the target plates [5-7]. The vacuum RMPs generated by external coils were calculated by the vacuum code ERGOS [11] and are imposed at the computational boundary (ITER wall), progressively increasing on a time scale of a few *ms*. The progressive switch on of the RMPs at the boundary was implemented for numerical reasons to avoid transient un-physical currents at the edge in the vacuum region. In the vacuum code ERGOS the horizontal parts of the RMP coils are approximated with curves and vertically with straight lines. In the ERGOS code, the upper (1) and low (2) corners of the coils were taken as follows: *upper row: R_1= 7.73m, Z_1=3.38m, R_2=8.26m, Z_2=2.62m; middle: R_1=8.62m, Z_1=1.79m, R_2=8.66m, Z_2=-0.55m; low: R_1=8.23m, Z_1=-1.55m, R_2=7.77m, Z_2=-2.38m.* The toroidal coordinates of the corners (the same for 1 and 2) of the 9 coils in each row are calculated as following: $\varphi_i^{(1)} = \Delta\varphi_{width}^{coil}(i-1) + \Delta\varphi_{shift}^{corner,coil}$; $\varphi_i^{(2)} = \varphi_i^{(2)} + \Delta\varphi_{width}^{coil}$; $\Delta\varphi_{shift}^{corner,coil} = \Delta\varphi_{shift}^{center,coil} - 0.5\Delta\varphi_{width}^{coil}$ and the toroidal width and shifts for the corresponding coils are: $\Delta\varphi_{width}^{coil}$ *=29.4°(upper), 20.9°(middle), 30.5°(low);* $\Delta\varphi_{shift}^{center,coil}$ *=30°(upper), 26.7°(middle), 30°(low), i=1:9.* The currents in the coils are calculated as: $I_i = I_C \cos[-N(\varphi_i^{coil} - \Delta\Phi^{coil})\cdot\pi/180]$, where I_C is the peak current, $\varphi_i^{coil} = \Delta\varphi_{shift}^{center,coil} + 40\cdot(i-1);$, N –is the main toroidal number of the RMP spectrum needed and the phasing between coils $\Delta\Phi^{coil}$ is taken from the linear MHD response of code MARS-F optimization studies, which maximized the magnetic displacement near the X-point [9,10]. Because of the different definition of the starting toroidal angle in MARS-F and ERGOS codes for the phase shift between coils we used the formula: $\Delta\Phi_{ERGOS}^{coil,temp} = \Delta\varphi_{shift}^{center,coil} - (\Delta\Phi_{MARS}^{coil} + 180°)/N$. The phase in

the middle coil is taken to be zero both in MARS-F and ERGOS codes, so that the relative phasing can be calculated using formula: $\Delta\Phi^{mid,new}_{ERGOS} = \Delta\Phi^{mid,temp}_{ERGOS} - k\cdot 360°/N$; $\Delta\Phi^{coil}_{ERGOS} = \Delta\Phi^{coil,temp}_{ERGOS} - \Delta\Phi^{mid,new}_{ERGOS}$; *k=1*. The optimum phasing for each scenario (except for the *12.5MA* "non- optimum" case which was done for comparison with linear and non-linear MHD codes, see Sec.6) are presented in Tab. 1. Both codes ERGOS and MARS-F were successfully benchmarked for vacuum modelling to ensure that the same RMP coils geometry and vacuum fields (not presented here) were used.

Scenario	IMAS Reference	N	$\Delta\Phi^{up}_{MARS}$	$\Delta\Phi^{mid}_{MARS}$	$\Delta\Phi^{low}_{MARS}$	$\Delta\Phi^{up}_{ERGOS}$	$\Delta\Phi^{mid}_{ERGOS}$	$\Delta\Phi^{low}_{ERGOS}$
15MA,Vtor(2)	131025_24	N=2	145°	0°	195°	110.8°	0°	85.8°
		N=3	200°	0°	140°	56.63°	0°	76.63°
		N=4	250°	0°	95°	30.8°	0°	69.55°
15MA,Vtor(1)	131025_23	N=3	200°	0°	140°	56.63°	0°	76.63°
12.5MA optimum	131039_0	N=3	215°	0°	120°	51.63°	0°	83.3°
12.5MA non-optimum	131039_0	N=3	135°	0°	25°	78.3°	0°	114.97°
10MA	131036_21	N=3	240°	0°	110°	43.3°	0°	86.63°

Tab.1 RMP coils phasing for different ITER scenarios used in modelling.

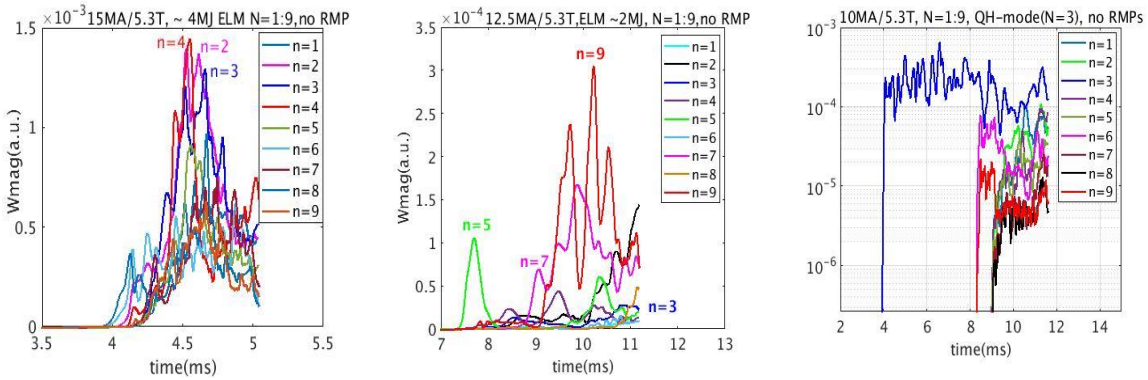
The resistivity, poloidal viscosity $\eta, \nu_\perp = \eta_0, \nu_{\perp 0}(T_e / T_{e,0})^{-3/2}$ and parallel Spitzer heat conductivity $K_\parallel = K_{\parallel,0}(T_e / T_{e,0})^{5/2}$ are temperature dependent in JOREK [7, 14]. In the present modelling the central perpendicular heat and particle diffusion were take *~10^{-6}* in normalized JOREK units [see for normalization 13-14], which corresponds to *~1.3m^2/s* in SI units. The diffusion is decreased in the pedestal region to keep the H-mode profiles without ELMs and RMPs [4-7]. The normalized parallel diffusivity is $\nu_\parallel = 10^{-5}$ (*~13m^2/s in SI*), the normalized parallel heat conductivity was taken $K_{\parallel,0} \sim 8\times 10^5$ *(~4x10^5 kg/m/s* in SI*)*. However, the Spitzer expression is valid only for high collisionality plasmas, so it was corrected for the central plasma by a kinetic flux limit (here we used $K_{//,\max} = 10$) similar to [12]. In the current source, the bootstrap current was evolved self-consistently in time depending on profile evolution as described in [13]. All dissipation parameters are rather close to realistic experimental values except the normalized resistivity $\eta_0 = 10^{-7}$, which was about of two orders higher (because of state-of-art numerical limitations for ITER-sized machine) if calculated for central ITER values in the *15MA* scenario.

3. MODELING OF NATURAL ELMs WITHOUT RMPs

For each ITER scenario considered, the stationary equilibrium with flows was obtained first on few *ms* time scale including only the *N=0* harmonic [7], then natural ELMs were modelled by adding the *N=1:9* harmonics initially at the noise level. The magnetic energy of natural ELMs for *15MA(Vtor2) 12.5MA, 10MA* scenarios are presented in Fig.2. Note that in the *15MA* scenarios the low *N* harmonics (*N=2,3,4*) are the most unstable (Fig.2a). In the *12.5MA* scenario the precursor *N=5* is followed by triggering of the most unstable *N=7,9* harmonics (Fig.2b). In the high beta *10MA* scenario the *N=3* harmonic remains the most unstable at the edge with QH-mode like behavior without ELM crashes (Fig.2c). The density and the maximum divertor heat flux during a natural ELM for *15MA 12.5MA* scenarios are presented in Fig.3. The total thermal energy loss in ELMs was *4MJ* and *2MJ* respectively (Fig.3-a,b). The two fluid diamagnetic effects and toroidal rotations included in the model were found to be the most important factors in explaining the experimentally observed rotation of the ballooning modes before the ELM crash and in the inter-ELM phase [6, 14]. In the *10MA* scenario the main *N=3* QH-mode like structure also rotates in the electron diamagnetic (or *E*x*B*) direction (Fig.4).

4. MODELLING OF ELMs WITH RMPs N=2,3,4 IN 15MA/5.3T SCENARIO.

The RMP current threshold studies were done for the *15MA/5.3T* scenario. The magnetic energies of the modes *N=1:9* during application of *N=3* RMPs with different maximum RMP coils currents (from *0kAt* to *60kAt)* are shown in Fig.5. Here the initial time without RMP was the same, but the harmonics energies are plotted here artificially shifted in time just for a better visual representation. One can see that for an RMP coil current larger than *45kAt*, the magnetic energy of RMPs (*N=3* harmonic) and the non-linearly most strongly coupled harmonics (*N=6,9*) are dominant. The other harmonics remain at a low noise level.



(a) ***(b)*** ***(c)***

Fig.2.Magnetic energy of N=1:9 harmonics in natural ELMs in 15MA (a), 12.5MA (b) and 10MA (c) scenarios.

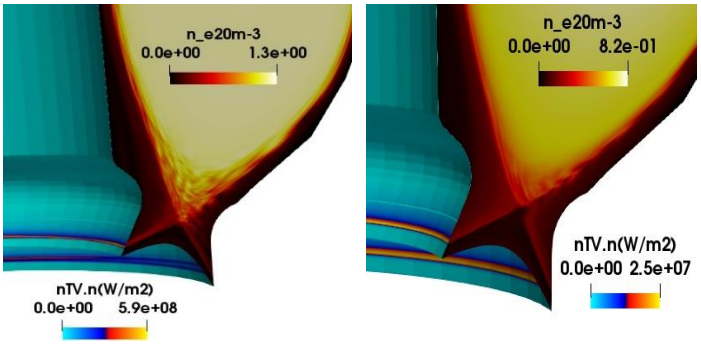


Fig3 The density and divertor maximum heat flux during a natural ELM N=1:9 for 15MA (left) 12.5MA (right) scenarios.

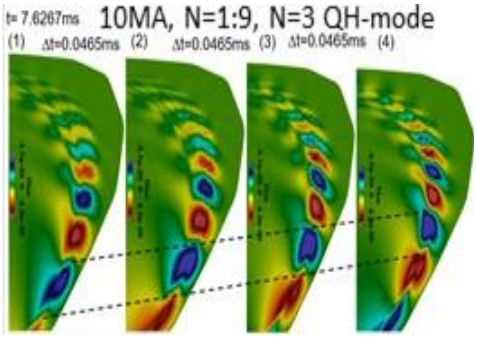


Fig.4. Rotation of the N=3 QH-mode like structure in the electron diamagnetic direction in 10MA scenario.

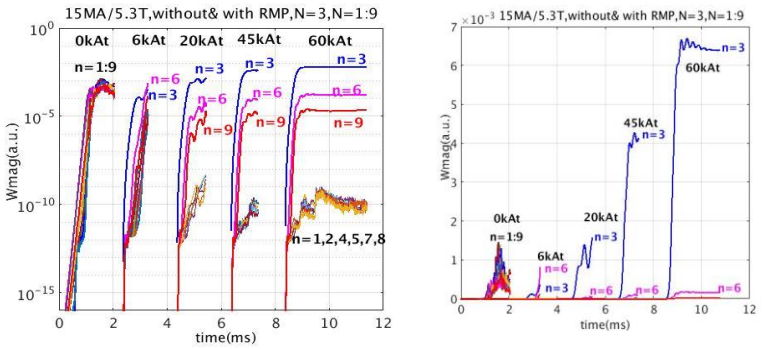


Fig.5. Magnetic energy of N=1:9 harmonics without and with RMPs in log scale (left) and linear scale (right) at 0-60kAt maximum currents in RMP coils.

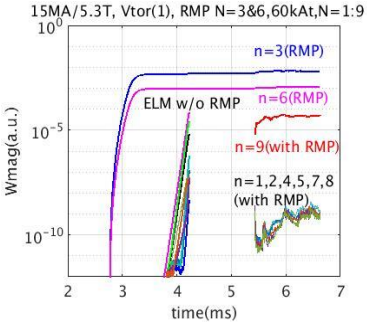


Fig.6. Magnetic energy without/with RMPs N=3&6 at 60kAt in 15MA scenario with increased rotation Vtor(1)

This corresponds to ELM suppression picture similar to one found in [5,6]. For lower RMP currents (*<45kAt*) the growth rates are usually decreased by RMPs, however the ELMs harmonics remain unstable, growing continuously and eventually produce an ELM crash. In the *15MA/5.3T* scenario with increased toroidal rotation (Fig.1 left) very similar results of ELM suppression were obtained (Fig.6). Here only the initial stage of an ELM without RMP is shown (with increased rotation the most unstable modes were *N=6,7,8*). For the case with RMPs we used two harmonics *N=3,6* in the RMP spectrum at *60kAt* and *N=1:9* modes were initialized when RMPs were established (Fig.6). The results of application of RMPs separately with *N=2, N=3, N=4* at maximum RMP current *60kAt* in *15MA* scenario are presented in Fig.7. Note that ELMs are strongly mitigated and crashes are avoided in all cases. The side harmonics *N*k*, where *N* is the main RMP harmonic number and k is integer are more strongly coupled to RMPs, are developing with RMPs but at lower level (Fig.7). Other side harmonics also are triggered via non-linear coupling and saturate, providing edge MHD turbulence instead of ELM crashes. Note that saturation level

is higher for *N=2* and *N=4* RMPs compared to the *N=3* case. The corresponding Poincare plots of plasma edge magnetic topology for *N=2,3,4* at the last time of the modelling are presented in Fig.8.As expected the magnetic energy (and edge ergodisation) of the main RMP harmonic at fixed current (here 60kAt) decreases with toroidal number *N*, since harmonics with higher poloidal numbers (*M*) are resonant at the edge ($q_{res}=M/N$) and the RMP perturbation decreases with a distance from the RMP coils approximately as $\sim 1/r^M$. Note characteristic lobes near X-point and narrow edge ergodic region typical for RMPs application pulses [5,6]. The plasma profiles in mid-

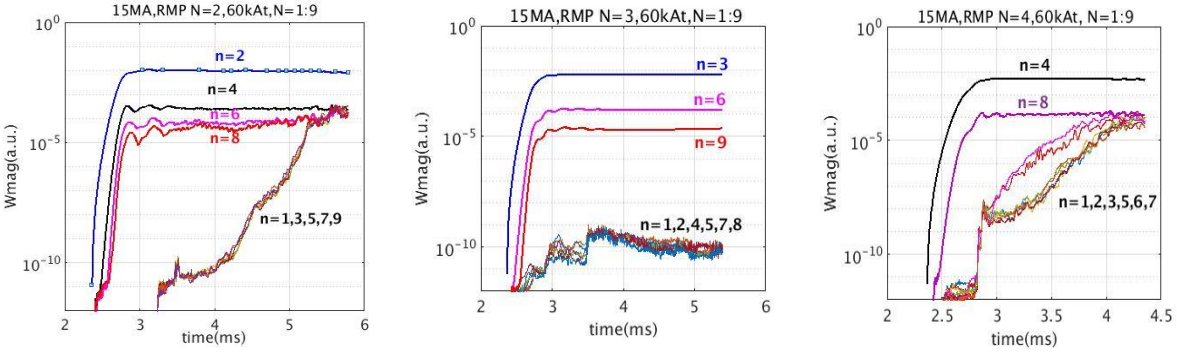


Fig.7. Magnetic energy of N=1:9 harmonics with RMPs N=2,3,4 (from left to right) at 60kAt.

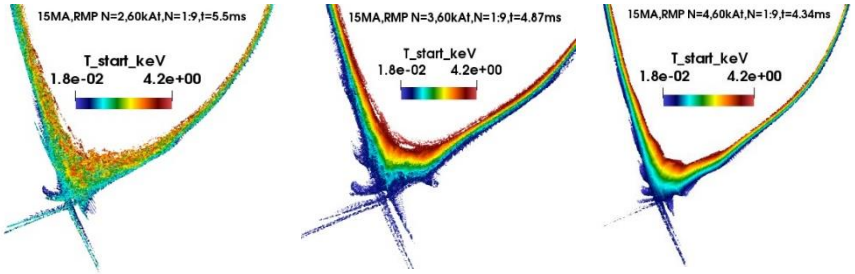


Fig.8. Magnetic topology for 15MA, with RMPs N=2,3,4 (left to right), 60kAt.

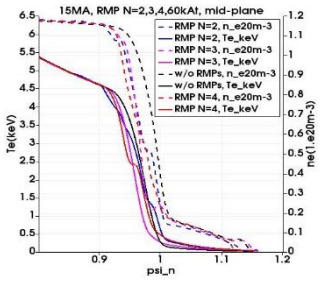


Fig.9.Plasma profiles for 15MA scenario with RMPs N=2,3,4, 60kAt. N=1:9.

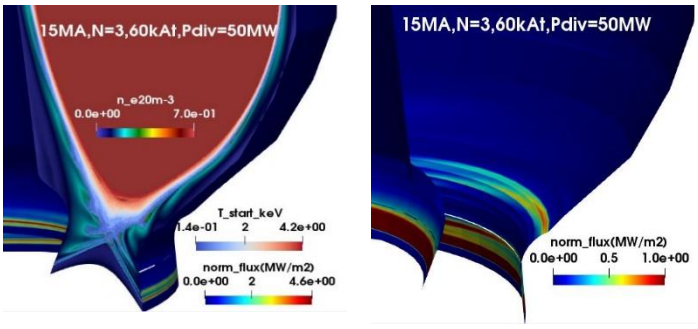


Fig.10. 15MA/5.3T scenario. Edge density, magnetic topology and normalized (considering power in divertor $P_{div,st}$=50MW, see Sec.7) stationary divertor heat flux with RMP N=3,60kAt (left) and normalized divertor and wall heat fluxes scaled to max 1MW/m^2(right).

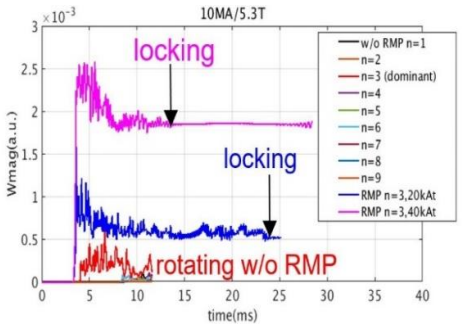


Fig.11. Magnetic energy without RMPs (N=1:9) and RMP N=3 at 20kAt,40kAt in 10MA/5.3T scenario.

plane with and without RMPs are compared in Fig.9. The energy transport slightly decreases with increased *N* of RMPs, but density transport is almost the same. The convective (*ExB*) density transport and conductive energy transport were observed in modelling with RMPs (Fig.10, left). Heat flux splitting was observed both in inner and outer divertor (see Sec.7 for more details). Note that at the Low Field Side (LFS) the largest heat fluxes remain in the divertor target and baffle decreasing further out from the initial strike point, however at the outer divertor baffle/first wall boundary heat fluxes *~1MW/m^2* are observed in modelling (Fig.10, right).

5. MODELLING OF ELMs SUPPRESSION BY RMPs N=3 IN 12.5MA,10MA/5.3T SCENARIOS.

The high beta *10MA* scenario is rather specific, since even without RMPs it exhibits features of a QH-mode without ELMs (Fig.2c), unlike the 12.5 MA scenario which resembles the 15 MA one. The application of RMPs at different RMP current amplitudes (*20kAt, 40kAt*) also lead to QH-mode like behavior (Fig.11). However the main *N=3* harmonic locks to the static RMP after few *ms* and the time of locking is larger for smaller RMP amplitude. (Fig.12 compared to Fig.4). The plasma profiles with RMPs are presented in Fig.13 showing strong density transport and almost no changes in temperature profile, which is typical for QH-modes. The magnetic energies of harmonics *N=1:9* with RMP *N=3* at *60kAt* in *12.5MA/5.3T* scenario are presented in Fig.14, where ELM suppression is also obtained. The plasma profiles in the mid-plane without/with RMPs are presented in Fig.15. Note the larger density transport compared to energy transport, which is observed also in many RMP experiments (Fig.16).

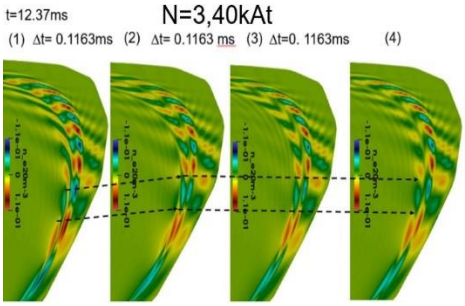


Fig.12. Transotion from rotation to locking to static RMPs N=3,40kAt in 10MA scenario

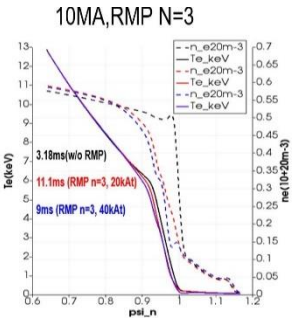


Fig.13. Plasma profiles with RMPs in 10MA scenario

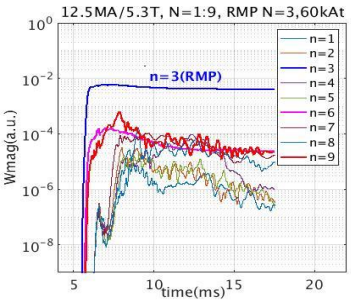


Fig.14. ELM (N=1:9) suppression at 12.5MA, RMP N=3,60kAt

6. DISPLACEMENT NEAR X-POINT WITH LINEAR (MARS-F) AND NON-LINEAR (JOREK) PLASMA RESPONSE

In linear MHD studies with MARS-F code it was found that the external kink-peeling plasma response is an important factor for ELM suppression by RMPs [9]. At present, the maximum perpendicular magnetic surface displacement near X-point with linear MHD plasma response gives better predictions for ELM suppression in experiment [9] compared to the initial vacuum criterion of edge islands overlapping [2]. The non-linear modelling [5] also pointed out on the role of the external kink plasma response in ELM suppression. Since the RMP coils phasing was optimised according to MARS-F criterion [10], it is interesting to compare displacements in linear and non-linear MHD codes. Note however that properly speaking the magnetic displacement is difficult to define in non-linear MHD especially when edge magnetic field is ergodic. Here we define the displacement in non-linear MHD as: $\xi_\perp \approx \delta T_e / (\partial T_e / \partial \psi)$ also used in [15], where δT_e is electron temperature perturbation, ψ is poloidal magnetic flux For the scenario *12.5MA/5.3T* with optimum phasing according to MARS-F, the displacement near the X-point at the last closed flux surface ψ_n*~0.99* was about *~7mm* at *60kAt* (Fig.17 is done for *30kAt* RMP current). With non-optimum phasing (Tab.1) the same displacement can be obtained by MARS-F simply by increasing the RMP current amplitude up to *~80kAt* , since MARS-F is a linear code (Fig.17). These values were very similar in JOREK modelling at early time (<6.2ms) when the single RMP harmonic N=3 is established: *~6mm* for optimum phasing at *60kAt* and *~8mm* for the non-optimum phasing at *80kAt* (Fig.18). However, usually in the later non-linear stage (here *>17ms*) with multi-harmonics and self-consistently changing plasma profiles the displacement in non-linear MHD is much larger (*~60mm*, not shown here) than in the linear MARS-F code.

7. DIVERTOR FOOTPRINTS

One important consequence of RMP application is the complex magnetic topology and splitting of the separatrix into a set of manifolds, seen in experiment as helical “lobes” at the X-point [2,3]. Crossing the divertor plates they form non-axisymmetric heat and particle fluxes which potentially can represent an issue for ITER, leading to local “hot spots” and material erosion. Rotation of the RMP field thus was considered as an option to smear out heat and particle fluxes, but as a drawback it could lead to significant mechanical stresses in RMP coils. Here we access the heat and particle fluxes without rotation of the RMP fields. Note also that in the present model many essential divertor physics such as kinetic neutrals, recycling, pumping, etc., are missing. However the localization of divertor heat and particle fluxes with self consistently modelled RMPs with plasma response can be estimated here. The modeling time for all scenarios (~few tens of *ms*) is short compared to ITER confinement

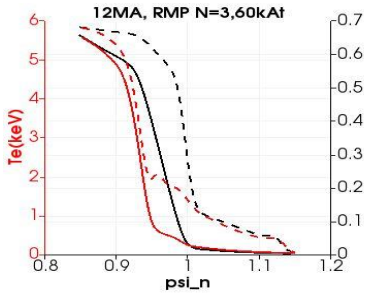


Fig.16. Plasma profiles for 12.5MA scenario with RMPs N=3, 60kAt, N=1:9.

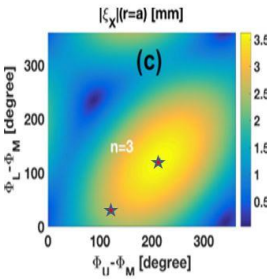


Fig.17. 12.5MA. MARS-F displacement, ψ_n~0.99, RMP N=3,30kAt, 12.5MA

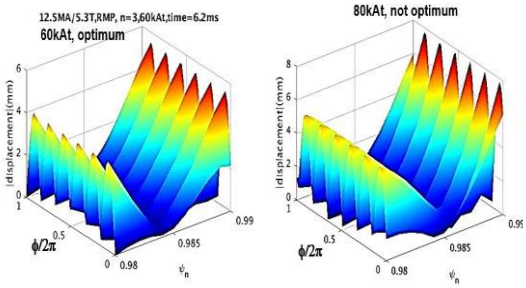


Fig.18. JOREK displacement near X-point (ψ_n~0.99) at optimum phasing (left) with single RMP N=3,60kAt and non-optimum phasing (right) at N=3,80kAt in 12.5MA scenario.

time (*>3s*), which is not presently accessible due to the computer time requirements for the small Alfven-like time steps needed in the non-linear multi-harmonics MHD modelling with JOREK code, even with a fully implicit scheme [4]. The extrapolation of heat fluxes to the stationary situation is done here using a normalization of the divertor heat fluxes with $P_{div,st}=50MW$ power going to the divertor and walls based on the assumption that approximately 66% of the total heating power (including fusion power) will be radiated in the core plasma and SOL+divertor in high Q ITER scenarios [8]. The extrapolation to the stationary situation when the time derivative of thermal energy is zero : $dW_{th}/dt=0$ is done by multiplying actual non-stationary perpendicular to the divertor target-baffle and first wall heat flux $P_{div,nst} = (T \cdot n_e \cdot \vec{V}) \cdot \vec{n}$ by a factor $P_{div,st}/P_{div,nst}$ ($\vec{n}$ is a normal to the surface vector, $T=T_e+T_i$). The normalized heat fluxes versus toroidal angle along the divertor length for the *15MA* scenario without RMPs and with RMPs *N=2,3,4* at *60kAt* are presented in Fig.19. Here the uppermost point at the inner divertor baffle is taken as zero length along divertor $L_{div}=0$ and the lowest point of the outer divertor is at $L_{div}=0.411m$. The non-normalized particle fluxes at the last time of modelling are presented in Fig.20. Note increased particle fluxes with RMPs, however not-stationary here. One can see that the splitting of the footprints in the *15MA/5.3T* scenario exhibits the *N*-symmetry of the main RMP harmonic (Fig.19,20). A footprint radial extension of *~20cm* was observed in the inner divertor and of *~40 m* in the outer divertor. At the *LFS* the peak heat fluxes with RMPs decrease from the initial strike point value remain in the divertor target/baffle areas. Note, however, that at the outer divertor baffle/first wall boundary the heat flux can remain as high as $\sim 1MW/m^2$ in stationary conditions (Fig.10). This could be a potential concern for first wall loads at the start of ELM suppression, since the switch-on of the RMP coils leads to a partial loss of confinement (up to *20%* in experiments [2]), so that heat fluxes to plasma facing components will transiently increase before a new stationary situation with RMPs is reached. This fact should be considered when RMPs are applied with more favorable application before or soon

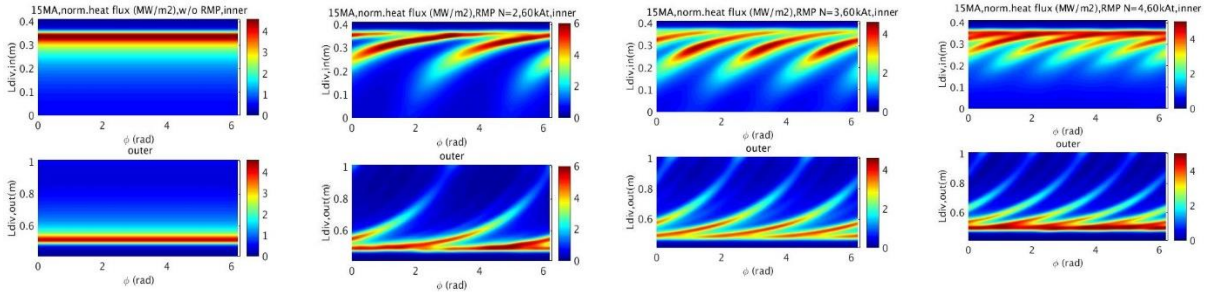


Fig.19. Normalized heat fluxes in 15MA scenario without and with (from left to right) RMPs N=2,3,4 at 60kAt.

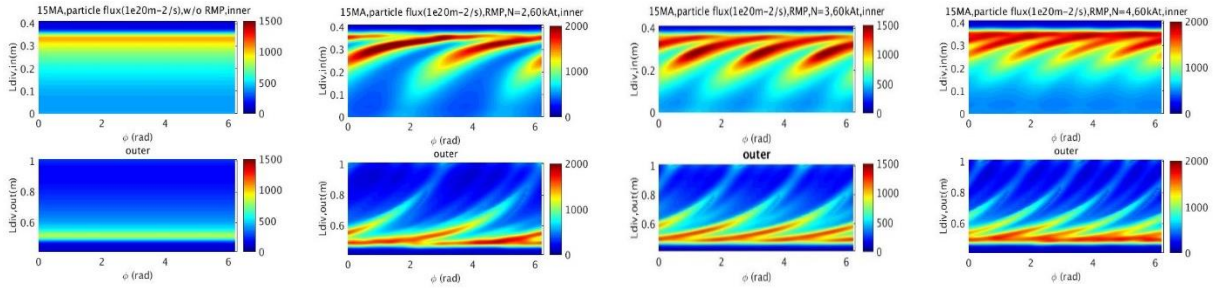
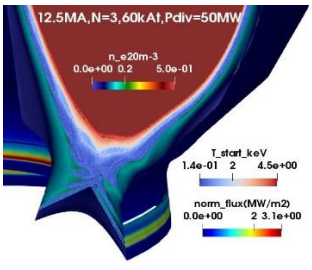


Fig.20. Particle fluxes in 15MA scenario without and with (from left to right) RMPs N=2,3,4 at 60kAt.

after the L-H transition, although optimization is required to avoid increasing the L-H power threshold with RMPs. Modelling of such conditions is out of scope of the present paper. The stationary normalized ($P_{div,st}$=*50MW*) heat fluxes in *12.5MA* and *10MA* scenarios are presented in Fig.21-22. Note that in the *10MA* scenario no clear splitting in inner divertor was observed (Fig.22). Similar to the *15MA* scenario (Fig.10 right) heat fluxes at the outer divertor baffle/first wall interface reach *~1MW/m*^{2} in stationary RMP regime in *12.5MA* and *10MA* scenarios.(Fig.21, 22 right)



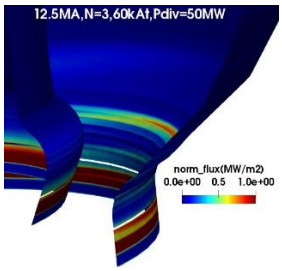
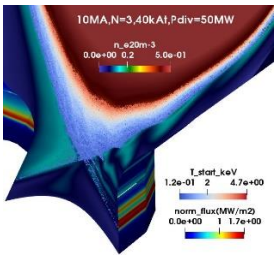


Fig.21. Divertor normalized heat flux and edge magnetic topology (left), heat flux on the diveror-wall (right) scaled to max 1MW/m^2*, 12.5MA, RMP N=3,60kAt.*



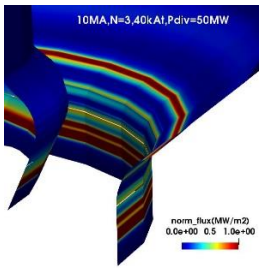


Fig.22. Divertor normalized heat flux and edge magnetic topology (left), heat flux on the divertor-wall (right), 10MA , RMP N=3,40kAt.

8. CONCLUSIONS

The interaction of ELMs with RMPs was studied in multi-harmonic non-linear MHD simulations for ITER scenarios *15MA,12.5MA,10MA/5.3T*. The RMP spectrum, optimized by the linear resistive MHD MARS-F code, with the main toroidal harmonics *N=2, N=3* and *N=4* were used (Tab.1). In the *15MA* scenario, the threshold for ELM suppression was found to be at an RMP coil current of *~45kAt-60kAt,* compared with a maximum coil capacity of *90kAt*. RMPs non-linearly generate a continuous MHD turbulent transport stabilizing ELMs in all scenarios. In the high beta poloidal *10MA/5.3T* steady-state scenario without RMPs an *N=3* rotating QH-mode was observed. With *N=3* RMPs (at *20kAt, 40kAt*), the mode is locking to the static RMPs in this scenario. The 3D divertor heat and particle fluxes demonstrate typical splitting with the main toroidal symmetry of the RMP spectrum. The radial extension of the 3D heat fluxes at maximum RMP coils current *60kAt* is about *~20 cm* at the inner divertor and *~40cm* at the outer divertor with the heat fluxes decreasing further out from the strike point from *~5-6MW/m*^{2} reaching *~1MW/m*^{2} at the outer divertor baffle/first wall interface in the stationary RMP regime (assuming a total power to the divertor/first wall of *~50MW*). Note that at the *LFS* heat fluxes with RMPs mainly remains within the divertor target/baffle area and within the design limits for divertor target (*<10MW/m*^{2}), baffle (< 5 MW/m^2) and first wall (*~1MW/m*^{2}). However in transient regimes when RMPs are switched on, part of plasma thermal energy is lost and these heat fluxes can be much larger; optimization of RMP switch-on needs to be studied further with respect to the ensuing power fluxes and L-H access.

ACKNOWLEDGEMENTS. The authors would like to thank the whole JOREK Team for collaborations and fruitful discussions. Part of this work has been carried out within the framework of the EUROfusion Consortium and has received funding from the Euratom research program 2019-2020 under grant agreement No 633053 and the ITER IO Contract No. IO/19/CT/ 4300001845. The views and opinions expressed herein do not necessarily reflect those of the European Commission. ITER is the Nuclear Facility, INB No. 174. The views and opinions expressed herein do not necessarily reflect those of the ITER Organization. This publication is provided for scientific purposes only. Its content should not be considered as commitments from the ITER Organization as a nuclear operator in the frame of the licensing process. This work was carried out the Marconi-Fusion supercomputer operated by CINECA

REFERENCES

[1] A Loarte A. et al Plasma Phys. Contr. Fusion 45(2003)1549
[2] M Fenstermacher et al Phys of Plas 15(2008) 56122
[3] R Hawryluk et al. Nucl. Fus 49(2009) 065012
[4] G T A Huysmans et al Plasma Phys Control Fusion 51 (2009) 124012
[5] F Orain et al Phys. Plasmas 26(2019), 042503
[6] S K Kim et al Nucl. Fusion 60(2020), 026009
[7] F Orain et al Phys of Plasmas 20(2013)102510
[8] A.R. Polevoi et al Nucl. Fusion 45 (2005)1451
[9] Y Liu et al Plasma Phys. Control. Fusion 58(2016)114005
[10] Y Liu et al this conference
[11] M Becoulet et al Nucl. Fusion 49 (2009) 085011
[12] M Becouet et al Nucl. Fusion 45 (2005)1284
[13] S Pamela et al Nucl Fusion 57(2017)076006
[14] M Becoulet et al Nucl. Fusion 57 (2017) 116059
[15] JK.Park et al., 62APS(2020, Nov.9-13) VP14:14